Geomorphology 214 (2014) 148–156

Contents lists available at ScienceDirect

Geomorphology

journal homepage: www.elsevier.com/locate/geomorph

Simulation of braided river elevation model time series with multiple-point statistics

Guillaume Pirot *, Julien Straubhaar, Philippe Renard

Centre for Hydrogeology and Geothermics, University of Neuchâtel, rue Emile Argand 11, CH-2000 Neuchâtel, Switzerland

ARTICLE INFO

Article history:
Received 30 July 2013
Received in revised form 24 January 2014
Accepted 28 January 2014
Available online 13 February 2014

Keywords:
Braided river
Topography
Modeling
Digital elevation model
Multiple-point statistics
Time-series

ABSTRACT

A new method is proposed to generate successive topographies in a braided river system. Indeed, braided river morphology models are a key factor influencing river–aquifer interactions and have repercussions in ecosystems, flood risk or water management. It is essentially based on multivariate multiple-point statistics simulations and digital elevation models as training data sets. On the one hand, airborne photography and LIDAR acquired at successive time steps have contributed to a better understanding of the geomorphological processes although the available data are sparse over time and river scales. On the other hand, geostatistics provide simulation tools for multiple and continuous variables, which allow the exploration of the uncertainty of many assumption scenarios. Illustration of the approach demonstrates the ability of multiple-point statistics to produce realistic topographies from the information provided by digital elevation models at two time steps.

1. Introduction

Braided rivers constitute an important part of alluvial systems in alpine regions such as Switzerland. Many of these rivers were channelized in the past and are now targeted by restoration projects (Glenz, 2013) for flood prevention, water management purposes, biodiversity preservation, and leisure activities (FOEN, 2009; Peter, 2009), particularly in the context of climate change (Macklin and Rumsby, 2007). As a result of the erosion and deposition processes, the morphology of braided rivers is a signature of such active systems. Morphology is a key parameter, first toward the understanding of dependent ecosystems (Amoros and Bornette, 2002; Richards et al., 2002; Clarke et al., 2003; Van Der Nat et al., 2003; Tockner et al., 2009), and also to better understand the main geological structures of the resulting aquifers in order to study groundwater flow and transport (Thomas and Nicholas, 2002; Käser et al., in press), or surface and subsurface relationships. In a hydrogeological context, simulations of successive morphologies could also be used to produce three-dimensional heterogeneous geological models. These issues are not addressed in this paper but they justify the need of topography models. The purpose of this work is to present a new way of modeling braided river topography and its evolution.

Static models of braided river morphology can be achieved by LIDAR data acquisition followed by image processing (Westaway et al., 2003) and analyses can be derived from descriptive methods characterizing the length scale and the main topographic structures (Rust, 1972; Miall, 1977; Germanoski and Schumm, 1993; Goff and Ashmore, 1994; Warburton and Davies, 1994; Foufoula-Georgiou and Sapozhnikov, 2001; Hundey and Ashmore, 2009; Lane, 2009). But these approaches are often limited to a single time step (static aspect) and restrained to the area of acquired data.

Simulations based on process imitating methods such as cellular automata models (Murray and Paola, 1994; Nicholas et al., 2009) or such as event-based models (Pyrcz et al., 2009), which can be validated by comparisons to laboratory experiments (Ashmore, 1982), allow for models of the system over successive time steps. Nevertheless, the conditioning to field measurements such as borehole data is often very difficult. To overcome this drawback, an alternative is the use of MPS simulations. These techniques are nonparametric and allow for the reproduction of complex spatial features from a conceptual model called training image (TI), as well as to account for conditioning to field data. To our knowledge, multiple-point statistics (MPS) has not yet been used to simulate successive braided river morphologies. MPS has been introduced by Guardiano and Srivastava (1993), and first practical algorithms such as SNESIM (Strebelle, 2002) were designed for the simulation of categorical variables. The algorithm proposed by Mariethoz et al. (2010), the direct sampling (DS), is much more flexible and can deal with joint simulations of multiple categorical and continuous variables. Because the DS method can reproduce spatial structures and complex correlations between several continuous variables (Mariethoz et al., 2012), this algorithm allows for simulations of successive digital elevation models (DEMs).

* Corresponding author. Tel.: +41 32 718 26 07.
E-mail address: guillaume.pirot@unine.ch (G. Pirot).

http://dx.doi.org/10.1016/j.geomorph.2014.01.022
0169-555X/

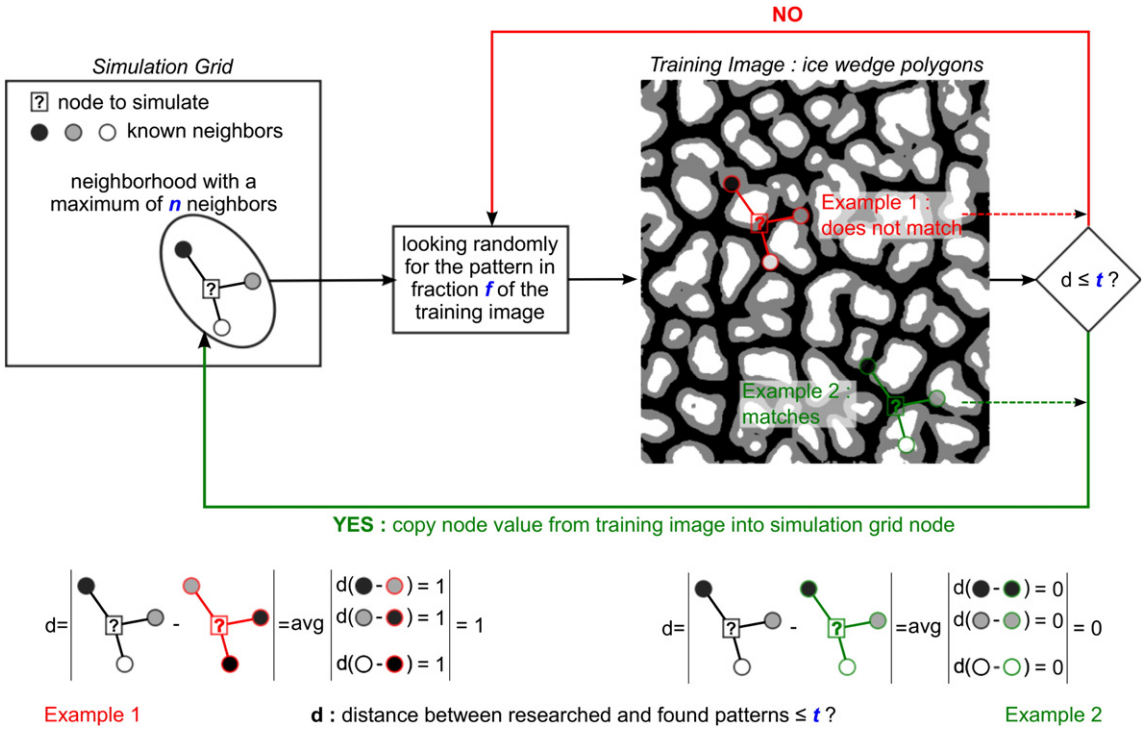

Fig. 1. Workflow of DS.
Courtesy of Meerschman et al. (2013).

Following those ideas, in this paper, the principle of a new method to simulate braided river topographies at successive time steps is proposed. It combines the advantages of the DS algorithm, with the large-scale data available from LIDAR topography. The approach is illustrated with statistical simulations of topography time series. The training datasets (TIs) are based on successive DEMs of the Waimakariri River, New Zealand (Lane et al., 2003) acquired with LIDAR at four time steps.

The paper is structured as follows. The DS algorithm is briefly presented in Section 2. The simulation of DEM time series with MPS algorithms is not straightforward, mainly because of large scale heterogeneities and trends in the TIs. Therefore Section 3 describes first a data analysis of the available TIs. That leads us to propose a methodology making use of auxiliary variables to enable realistic simulations of successive DEMs, with respect to the observed nonstationarities present in sparse training data sets. The method is detailed and demonstrated within Section 4. The paper ends with a statistical validation of the simulations in Section 5.

2. The direct sampling, an MPS algorithm

Multiple-point statistics (MPS) algorithms allow us to simulate a random function Z on a domain called the simulation grid. The random function spatial statistics are retrieved from a conceptual model known as TI. In the TI, Z is known over its entire domain (Fig. 1).

Each pixel of the simulation grid is simulated sequentially, one after another. A random path visiting every node in the simulation grid is defined, and each location $\mathbf{x}$ in the path is successively simulated as follows. The data event $\mathbf{d}(\mathbf{x})$ is the pattern constituted by the spatial ensemble of known values $Z(\mathbf{x}+\mathbf{h_i})$ in the neighborhood of $\mathbf{x}$ ($\mathbf{h_i}$ being a lag vector), i.e., the conditioning data and the already simulated points. Then, the value $Z(\mathbf{x})$ to simulate at location $\mathbf{x}$ is drawn from the cumulative distribution function F conditionally to the local data event $\mathbf{d}(\mathbf{x})$: $F(z, \mathbf{x}, \mathbf{d}(\mathbf{x})) = \text{Prob}\{Z(\mathbf{x}) \leq \mathbf{z}|\mathbf{d}(\mathbf{x})\}$. F is derived from a similar local data event present in the TI. F can be dealt with in two ways.

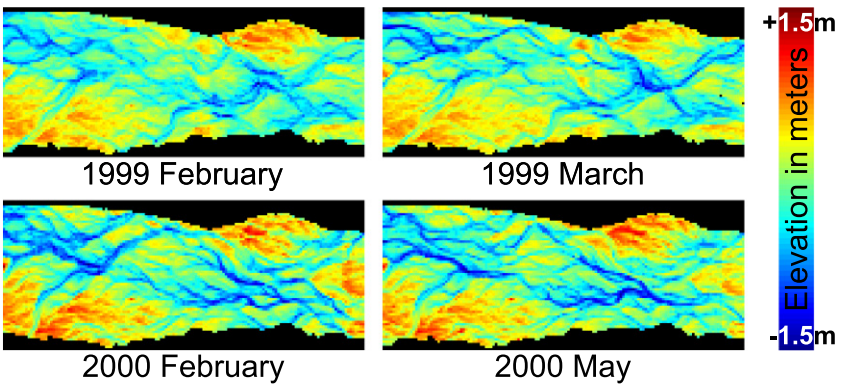

Fig. 2. 2,900 m × 1,200 m (145 pixels × 60 pixels — x axis × y axis) DEMs of the Waimakariri River, New Zealand at four time steps. Red: highest elevations; blue: lowest elevations.

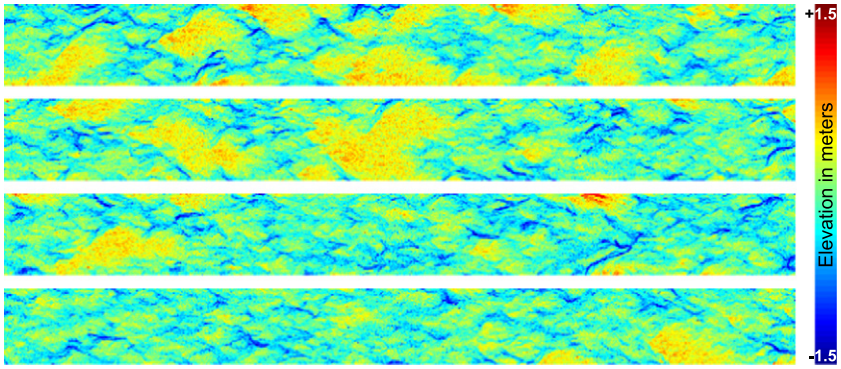

Fig. 3. 11,600 m × 1,200 m (580 pixels × 60 pixels) simulations of DEMs with DS, using a monovariate TI. Red: highest elevations; blue: lowest elevations.

The first efficient MPS approaches — implemented for instance by Strebelle (2002) in SNESIM or by Straubhaar et al. (2011, 2013) in IMPALA — rely on computing an histogram of the patterns present in the TI and compatible with the local data event **d**. These approaches are limited to categorical variables and with fixed search neighborhood templates. The use of successive multigrid simulation allows us, in that case, to capture and reproduce the structures from the TI at different scales while *using small search templates*, but may create some artifacts.

In a more recent approach, the DS algorithm (Mariethoz et al., 2010) skips the pattern histogram computation. Instead, for the simulation of a value at location **x** in the simulation grid, the TI is randomly scanned until a location **y** with a pattern $\mathbf{d}(\mathbf{y})$ compatible with the data event $\mathbf{d}(\mathbf{x})$ is found. Then, the value $Z(\mathbf{y})$ is simply pasted into the location **x**, and the simulation continues with the next node **x** in the random path. The data event retrieved from the simulation grid is made up, at maximum, of the N closest informed nodes. Then, the scale covered by the data event is large in the beginning of the simulation, and becomes smaller at the end, allowing the capture of structures within the TI at different scales. Specifying a normalized distance $D(\mathbf{d}(\mathbf{x}), d(\mathbf{y}))$ between patterns, the compatibility of two patterns is defined as follows: $\mathbf{d}(\mathbf{x})$ and $\mathbf{d}(\mathbf{y})$ are compatible if and only if $D(\mathbf{d}(\mathbf{x}), \mathbf{d}(\mathbf{y})) < t$, where t is a tolerance (or threshold) chosen by the user. Moreover, in order to reduce the computational time for the simulation of one node **x**, a maximal fraction f (chosen by the user) of the TI is scanned and, if a compatible pattern is not found, the value $Z(\mathbf{y})$ at the visited location **y** corresponding to the best match between $\mathbf{d}(\mathbf{x})$ and $\mathbf{d}(\mathbf{y})$ is assigned to **x**. For a categorical variable, the distance $D(\mathbf{d}(\mathbf{x}), \mathbf{d}(\mathbf{y}))$ is usually defined as the proportion of the nodes in the patterns having a different value. Normalized distances (of type L_1 or L_2 for instance) can be used to deal with a continuous variable. The algorithm is straightforwardly extended to the multivariate case: in a situation with m joint variables, the simulation proceeds by comparing m pair of data events. Fig. 1 illustrates the basic principles of DS. Further details about the DS algorithm can be found in Mariethoz et al. (2010)'s publications and additional examples of DS simulations are available in the papers of Mariethoz and Kelly (2011) and Meerschman et al. (2013).

3. Topography data analysis and description with auxiliary variables

In this section, we focus on the LIDAR data analysis, showing why it cannot be used directly as a TI, and how to overcome these issues.

3.1. DEM as training image

The DEM data used in this study were provided by Lane et al. (2003). This data set from the Waimakariri River was acquired between February 1999 and May 2000 at four different time steps as shown in Fig. 2. Originally, the data had a resolution of 1 m/pixel, and the elevation was the absolute elevation above sea level. In order to work with simulation grids larger than the TI, and to give as much importance to the change of elevation in both transversal and longitudinal directions, the main trend of the DEMs, i.e., their main slope, was removed. In other words, the average elevation computed over the longitudinal (x) axis is removed from the DEM. It means that for each x-coordinate (one column here), the average elevation is computed and subtracted to the measured elevation for all points of this x-coordinate. To speed up the MPS simulations, the resolution is coarsened by a factor of 20 ($\Delta X = 20 \times dx_{initial}$, $\Delta Y = 20 \times dy_{initial}$). The upscaling is done by averaging the local altitudes. It induces a smoothing of the data, but still respects the main topography structures from the original data (Lane et al., 2003).

Some simulations of DEMs with the DS algorithm, using directly the Waimakariri River DEMs (Fig. 2) as TI, are presented in Fig. 3.

We can observe that many structures of the topography present in the TI can be reproduced in the simulations. But an important drawback

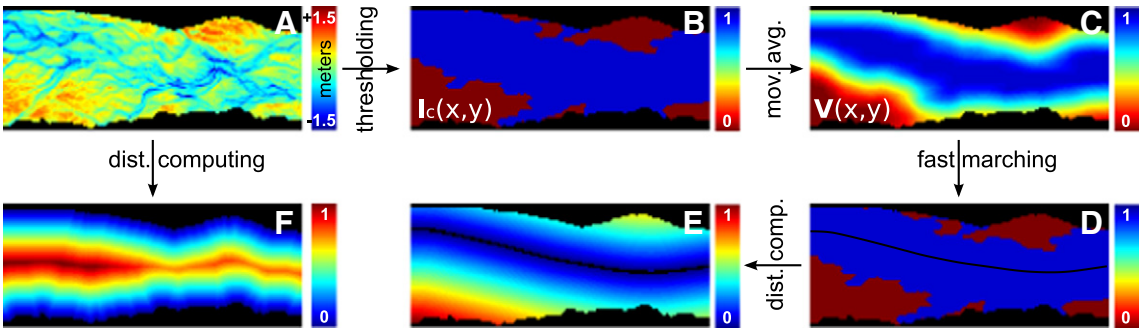

Fig. 4. Auxiliary variable workflow. (A) Initial DEM; (B) main channel; (C) velocity field; (D) main channel and its centerline; (E) normalized distance to the centerline; (F) normalized distance to the edges.

shows up: higher elevation parts in yellow or red and deeper channels in dark blue seem to be randomly located in the simulation grid. However, the higher parts are expected to be located on the sides of the domain. It is an observation that the human brain can deduce from the TI, but that the algorithm cannot infer automatically. This is a well known problem — the MPS algorithm assumes that the TI is stationary, meaning that any pattern present in the TI has the same probability to occur at any location. If this is not the case, special techniques must be applied. Nonstationarity in the TI can be overcome by using probability maps or auxiliary variables (Chugunova and Hu, 2008; Boucher, 2009; de Vries et al., 2009) in classical MPS algorithms such as SNESIM (Strebelle, 2002) or IMPALA (Straubhaar et al., 2011). With the DS algorithm, auxiliary variables can be used as well to guide the spatial positioning of the topography structures (Mariethoz et al., 2010).

3.2. Defining auxiliary variables

Looking at the DEM variable in Fig. 2, two main features can be distinguished: the less active part of the river is characterized by larger and higher elevation zones on the sides of the river, and the most active part of the river called the *main channel*, is characterized by deeper channels and small to medium elevation zones.

The main channel can be represented by its centerline. This allows us to compute a distance between each location in the river and this centerline. This first auxiliary variable — distance to the centerline — shall prevent to generate large and high elevation zones within the main channel. In addition, a distance can be computed between each location in the river and the river edges. This second auxiliary variable — distance to the edges — shall ensure the absence of channels or pools cutting one of the large and high elevation zones present on the edges. As illustrated in Section 4.2, these two distances will prove to be sufficient to help the algorithm localize the topography structures. Fig. 4 gives an overview of the process to compute the centerline and the auxiliary variables.

More details are available in the following paragraphs. The process is repeated for all available DEMs (Fig. 2).

3.2.1. Delineating a centerline in the main channel

The (x, y) coordinates system, used in what follows, refers to the x (longitudinal) and y (transversal) axes introduced in Section 3.1.

First of all, the main channel is delineated by thresholding the elevation in the DEMs. In our example, a threshold of 0.3 m is used. Zones above the threshold are post-processed to remove isolated groups or zones that are not adjacent to the edges. The result is an indicator function $I_c(x, y)$ locating the main channel when $I_c(x, y) = 1$, as shown in blue in Fig. 4B.

Then the centerline is obtained, by using a Matlab implementation of the fast-marching algorithm (Cao and Greenhalgh, 1994; Sethian, 1996; Peyré and Cohen, 2003). It consists in finding a least effort path — i.e. shortest distance path — in a velocity field between two points. The velocity field $V(x, y)$ (Fig. 4C) is obtained by averaging the main channel indicator function $I_c(x, y)$ with a 20 pixel radius moving window, $V(x,y) = \frac{1}{S} \times \int_S I_c(x,y)dS$. The starting point or inlet is defined on the left edge as the point of coordinate $Inlet_x = 0$ and $Inlet_y$ as the average of y for which $\max\{V(x, y), x = 0\}$ is reached. The ending point or outlet is chosen on the right edge as the point of coordinate $Outlet_x = 145$ and $Outlet_y$ as the average of y for which $\max\{V(x, y), x = 145\}$ is reached. The resulting centerline is displayed in Fig. 4D.

Now that both the centerline and the edges of the river are known, the auxiliary variables can be computed.

3.2.2. Distance to the centerline

The distance to the centerline is defined for each point of the TI as the minimum Euclidean distance between the considered point and all the points describing the centerline. It is then normalized by the maximum distance over the domain. The variable is displayed in Fig. 4E.

3.2.3. Distance to the edges

The distance to the edges is defined for each point of the TI as the minimum Euclidean distance between the considered point and all the points describing the edges. It is then normalized by the maximum distance over the domain. The variable is displayed in Fig. 4F.

4. Simulation of successive topographies

We proceed in three main steps to simulate successive DEMs.

The first step (Section 4.1) consists in defining the initial setup. It consists of:

- creating an initial centerline,
- simulating the river edges — these are then fixed across time and valid for the whole time-series and they determine the lateral size of the simulation domain for the topographies
- generating a successive centerline time-series,
- computing the associated auxiliary variables.

The second step (Section 4.2) is to simulate an initial topography. The third step (Section 4.3) is a Markov chain transition kernel that consists of simulating the topography at time step $n + 1$, with respect to the previously simulated topography at time step n. All simulations are obtained with the DS algorithm.

4.1. Test case setup

For this example, 100 time steps are considered for a two-dimensional topography simulation grid of 580 pixels × 84 pixels that corresponds to 11,600 m × 1680 m.

Edges and centerlines are two-dimensional features that can be described as one-dimensional variables as shown by Mariethoz et al. (in press). In our case, the centerline or the edges are described not as a succession of angles but as a succession of derivatives dy/dx for simplicity. This allows us to work on a fixed length of 580 pixels along the x-axis (longitudinal). The edge and centerline derivatives TI used for the following simulations are extracted from the four successive DEMs of the Waimakariri River (Fig. 2).

4.1.1. Creating an initial centerline and river edges

The first centerline is obtained by MPS simulation of its lateral derivative along the longitudinal axis. The cumulative sum of the derivatives gives the lateral coordinate for each point on the longitudinal axis of the grid.

The edges are similarly simulated with MPS but constrained loosely to some conditioning points. For the upper or the lower edges, we compute a straight line parallel to the linear approximation of the centerline but ensuring a minimum distance of 10 pixels with the centerline. Then for each edge, the conditioning points are the starting point, ending point, and 15 points uniformly drawn from the corresponding straight line. Once the edges are simulated, we consider them fixed and valid for all time steps. The width (y-axis) o f the simulation domain is then fixed to 84 pixels in our example.

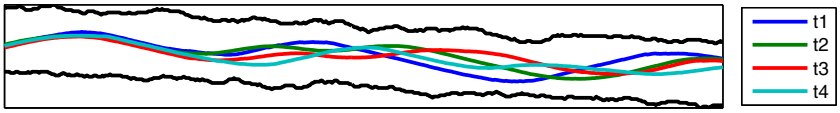

Fig. 5. Simulated edges and centerlines at four successive time steps for 580 pixel × 84 pixel simulations.

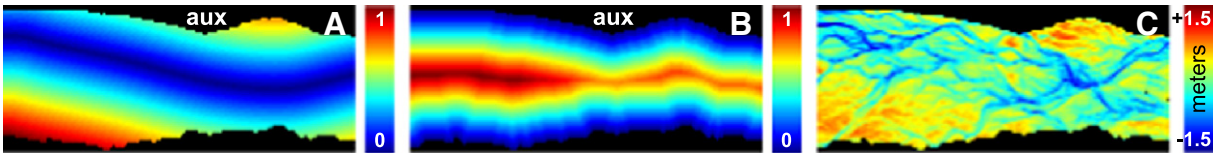

Fig. 6. Auxiliary variables (A, B) and variable of interest (C) for the TI; (A) distance to centerline, (B) distance to edges, (C) topography.

The conditioning of edge simulations to sampled points is obtained by using an iterative accept–reject algorithm. The sampled points are ordered as (P_i). Let us denote S_i the ith segment (i.e., part of a river edge) between P_i and P_{i+1}. The segments are successively simulated. To generate a segment S_i, successive derivatives are simulated and cumulatively added to obtain a line starting from P_i; then if the distance d_{i+1} between its ending point is too far from P_{i+1}, for instance $d_{i+1} \geq 2$ pixels, the simulation of S_i derivatives is rejected, and another one is launched, until it is accepted. When a segment S_i is accepted, the simulation continues with the simulation of the next segment, S_{i+1}, starting from the ending point of S_i. A resampling (of points P_i) is done if too many simulation attempts are rejected.

4.1.2. Generating a time-series of successive centerlines

Knowing the nth centerline, the lateral coordinates of both starting point and ending point are locally perturbed. Additional points are retained between the starting point and the ending point with a longitudinal interdistance uniformly drawn between 40 pixels and 100 pixels. Both lateral and longitudinal coordinates of these points are locally perturbed. The lateral perturbations are uniformly drawn in [−3 pixels, 3 pixels]. The longitudinal perturbations are uniformly drawn in [−5 pixels, 5 pixels]. All the perturbed points are used as conditioning data. Only centerlines that exist between the edges and with a minimum distance of 10 pixels to the edges are kept. If the simulation of the $n+1$th centerline is rejected, the nth centerline is sampled again and the $n+1$th centerline is resimulated. Fig. 5 illustrates the first four centerlines.

4.1.3. Computing auxiliary variables

Once edges and centerlines are defined, the fully informed auxiliary variables may be computed, as explained in Section 3.2.

4.2. Initial topography

To generate an initial DEM, a slope-free topography is simulated with the DS algorithm. The distance to the centerline and the distance to the edge variables are used as auxiliary variables. They are always exhaustively informed and guide the DS algorithm to localize the different kinds of structures of the variable of interest — the topography — in the realizations. The TI contains all DEMs for the available time steps (Fig. 2). As for each state, the topography is a two-dimensional data set; it results in a three-dimensional TI, the third dimension representing the time steps. Fig. 6 illustrates a 2D slice of the TI and its auxiliary variables at time step 'March 1999'.

The auxiliary variables — distances to the centerline and to the edges — are exhaustive for the simulations as shown in Fig. 7A and B.

Four possible realizations of DEMs with the same values for the exhaustive auxiliary variables (Fig. 7A and B) are displayed in Fig. 7C, D, E, and F. The parameters employed for the simulations with the DS algorithm are listed in Table 1.

As one can see, the different topography structures are well reproduced and well placed according to the edges and to the main active channel. Moreover, the exhaustive auxiliary variables do not constrain too much the simulation: with the same auxiliary variables, every realization is unique. So, the main active channel centerline and edges appear to

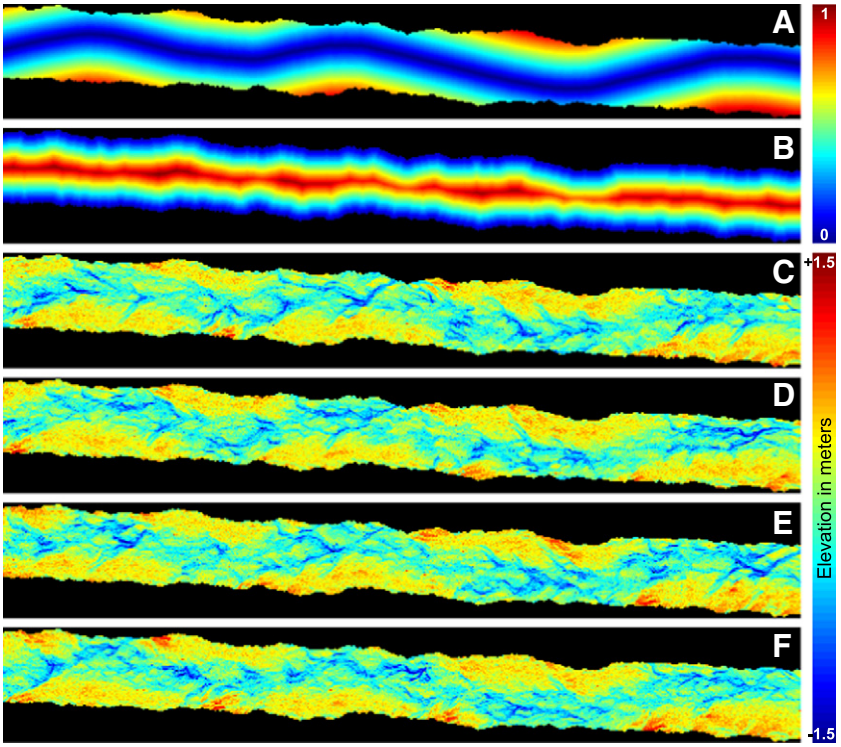

Fig. 7. Conditioning data: (A) distance to the centerline, (B) distance to the edges, and four DEM simulations (C), (D), (E), and (F) with a three variable TI.

Table 1
DS algorithm parameters for initial topography simulation.

Parameters	Value
Homothety	None
Rotation	None
Search neighborhood	30 pixels × 15 pixels
Maximum number of neighboring nodes	20 for auxiliary variables 30 for the simulated variable
Maximum density of neighboring nodes	0.1 for auxiliary variables 1.0 for the simulated variable
Type of acceptance distance	$L - 1$
Distance acceptance threshold	0.2 for the distance to centerline variable 0.15 for the distance to edge variable 0.05 for the simulated variable
Maximum scanning fraction for each TI	0.7
Post-processing	None

be sufficient to simulate realistic DEMs. A quantitative criteria to test the quality of the DEM simulations is proposed in Section 5.

4.3. Simulation of a topography conditional to a previous topography

The DS algorithm enables realistic simulations of DEMs using exhaustive auxiliary variables based on the given centerline and edges. As a consequence, the same auxiliary variables — distance to the centerline and distance to the edges — shall be kept to simulate successive DEMs. In order to simulate a DEM at time step $n + 1$ with respect to the previous DEM at time step n, the auxiliary variables are informed at two different time steps, n and $n + 1$; and an additional auxiliary variable providing the elevation in meters at time step n is considered. This results in the use of five exhaustive auxiliary variables along the variable of interest for the simulations, taking into account the evolution of the centerline and the evolution of the edges in addition to the evolution of the elevation. As illustrated in Fig. 8, the simulated variable (elevation at time step $n + 1$) in the training data set (Fig. 8) is the February 2000 DEM (C2). The five exhaustive auxiliary variables are the February 1999 DEM (C1) and the distance to the edges (B1 and B2) and the distance to the centerline (A1 and A2) both at time steps February 1999 and February 2000.

The parameters employed for the simulations with DeeSse are listed in Table 2.

Some examples of successive topography simulations are presented in Fig. 9B, C, D and E. The first DEM (Fig. 9A) is obtained with the simulation method described in Section 4.2. The following simulations allow us to model the evolution of the channels and of the side bars, grouping, diverging, or moving through time. Compared to the TI, the results are visually satisfactory. A statistical test of the successive DEM simulations is proposed in Section 5.

5. Statistical validation of topography simulations

This section is focused on the variable of interest: the elevation in meters, as the auxiliary variables are only used for guiding the simulation of successive DEMs. To test the quality of the simulated DEMs, they are compared to the TIs (Fig. 2) through (i) the empirical cumulative distribution functions (ECDF) regardless of the location (one-point statistics), and (ii) the gamma connectivity function (Renard and Allard, 2013) for testing the spatial organization of the structures.

Two-point statistics like variograms or multiple-point statistics such as spatial cumulants (Dimitrakopoulos et al., 2010) or statistics on patterns could also be used. However two-point statistics are not sufficient to characterize complex structures Guardiano and Srivastava, 1993; Gómez-Hernández and Wen, 1998. Multiple-point statistics are limited by the dimensions and the geometries of the retained neighborhood as well as by the necessity of discretizing continuous variables into categorical variables if the assessment is based on MPS histograms (Boisvert et al., 2010). The main reason why we use the gamma connectivity function is that the DEM simulations are intended to be used for solute transport and groundwater flow simulations. In this case, the reproduction of the connectivity patterns is crucial (Renard, 2007). Moreover, the connectivity function provides a global measure for the entire domain, and it can be computed over a continuous field such as the elevation in meters for instance.

The validation is performed for the two following cases. The initial topography simulations presented in Section 4.2 will be referred to as case (*A*). In this case, 100 realizations obtained with the same fully informed auxiliary variables are considered; the centerline and the edges are fixed for all the realizations. The successive topography simulations presented in Section 4.3 will be referred to as case (*B*). In that case, 100 realizations represent 100 successive time steps, and therefore have different fully informed auxiliary variables as the centerline evolves at each time step.

5.1. Empirical cumulative distribution function (ECDF)

To assess the quality of simulations from a one-point statistics point of view, we compare the elevation variable ECDF of the TIs in black with those of the realizations in gray in Fig. 10.

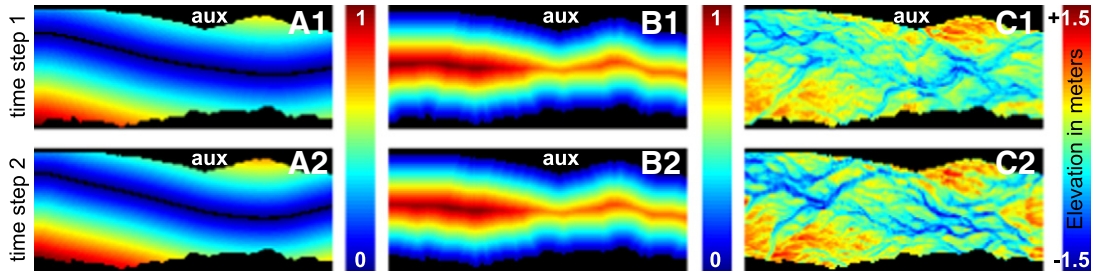

Fig. 8. TI and its five auxiliary variables to simulate successive topographies: distance to centerlines A1 at time step 1 and A2 at time step 2; distance to edges B1 at time step 1 and B2 at time step 2; elevations (in meters) C1 at time step 1 and C2 at time step 2.

Table 2
DS algorithm parameters for successive topography simulations.

Parameters	Value
Homothety	None
Rotation	None
Search neighborhood	30 pixels × 15 pixels
Maximum number of neighboring nodes	20 for distance variables 30 for elevation variables
Maximum density of neighboring nodes	0.1 for auxiliary variables 1.0 for the simulated variable
Type of acceptance distance	$L-1$
Distance acceptance threshold	0.2 for distance auxiliary variables 0.15 for the elevation auxiliary variable 0.05 for the simulated variable
Maximum scanning fraction for each TI	0.7
Post-processing	None

The first thing to notice is that in the TIs, the ECDFs are close but not identical for the four available time steps. These differences can be explained because the centerlines are slightly different, which induces a different distribution of the nonstationarities. Another reason is that these time steps are part of some cycles in the evolution of the braided river: the topography is slightly but constantly eroded between two floods, but each flood event is a way of resetting the topography distribution (Lane et al., 2003).

Seemingly the ECDFs are better reproduced in case (*B*) than in case (*A*). The main reason for it, again, is a difference in the localization of the nonstationarities. As in case (*A*), the centerline is the same for the 100 realizations, it does not offer as much exploration possibilities in the TIs as in case (*B*) where the centerlines are different.

5.2. Gamma connectivity indicators

As previously discussed, the gamma connectivity function defined by Renard and Allard (2013) is used to check the quality of the pattern reproduction. Given an indicator variable I, its gamma-connectivity measure, Γ_I, is defined as the probability that two points belonging to the medium $I=1$ are connected. In our situation, this connectivity measure is computed on indicator variables obtained by thresholding the simulated altitude field at several levels. Each threshold τ defines two complementary zones: a lower level (zone 1) below the threshold and an upper level (zone 2) above the threshold. The gamma connectivity, $\Gamma_{\tau,z}$, is then defined for each threshold level τ and zone $z \in \{1,2\}$ as the proportion of connected pairs of points belonging to z regarding the number of pairs of points in z. Results are displayed in Fig. 11.

For both cases (*A*) and (*B*) as well as for both zones, the simulations have a gamma connectivity function quite close to the reference gamma connectivity functions of the TIs: the jumps in the connection proportions take place at the same range of thresholded values and have the same amplitude. The quality of the realizations in terms of connectivity may then be considered as fulfilled.

6. Discussion and conclusion

The models presented above reproduce the spatial statistics of braided river elevation at successive time steps. The proposed method allows the generation of models showing a realistic evolution of the bars and channels, while it is not based on direct physical processes. We have shown that with a relatively small training data set, the DS algorithm successfully simulates the successive time-related DEMs, using exhaustive auxiliary variables that help localize structural nonstationarities. Variable transformation allows reducing the complexity of the problem and gives satisfactory results within really short computing times, especially when transforming a two-dimensional variable such as a centerline or edges into a one-dimensional variable.

The statistical validation of the models is based on the comparison of connectivity functions as it is of main concern for flow and transport modeling. A comparison of computing requirements and similar or other statistics with cellular automata and event-based models could also be performed for further performance testing and validation.

The successive DEMs are simulated under the assumption that the simulated edges and the simulated centerlines are valid themselves. The initial centerline simulation can be considered valid as it is simulated with a TI derived from braided river centerline interpretation. The way of constructing the edges might seem artificial, but in real case studies, edges can be easily delimited through aerial photography. Furthermore, their evolution is usually much slower than the topography or the centerlines. Similarly, the way centerline perturbations are created seems artificial too. Here, as no additional information was available from the field, random perturbations were used to simulate their evolution. Acquiring more field data about centerline evolution over decades

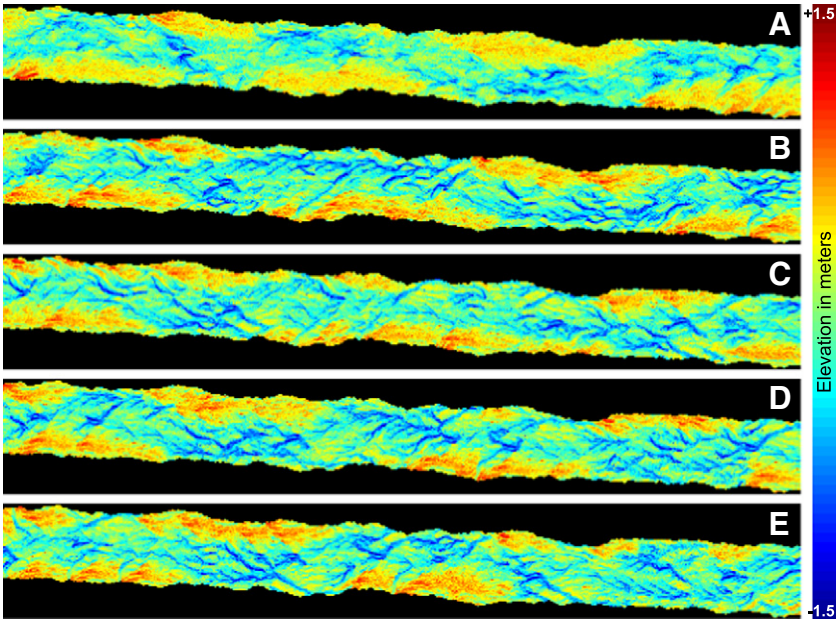

Fig. 9. Realization of five successive topographies: (A) initial DEM at time step 1; (B), (C), (D), and (E) successive DEMs at time steps 2, 3, 4, and 5, respectively.

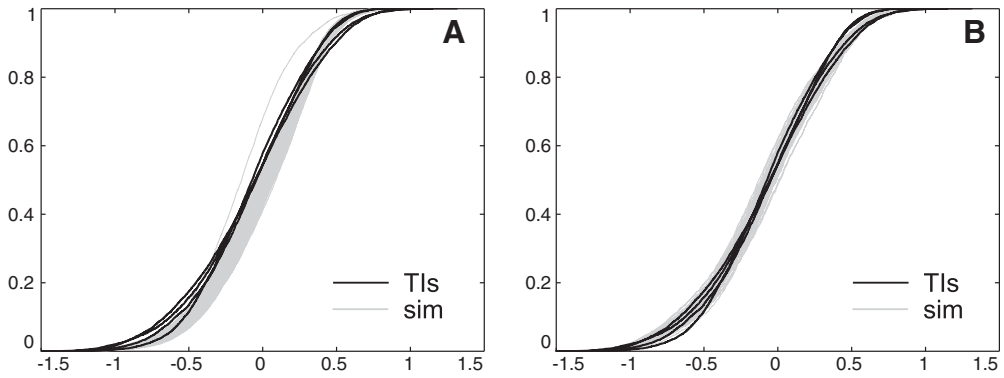

Fig. 10. ECDF of the elevation variable; comparison between the TIs (black) and the simulations (gray), for cases (A) and (B).

would be possible through low resolution aerial photography time series, which are not as expensive as high resolution LIDAR data acquisition. Having these data, it would be straightforward to model their evolution using the same statistical principle used here for the topography.

Finally, the simulation of DEM time series opens a wide range of perspectives in the fields of water-related risk management and braided river aquifer modeling. Indeed such aquifers are built by successive erosion and deposition processes affecting geological records and surface morphology. Stacking up successive topographies could enable us to mimic the erosion and deposition steps and allow simulating the main internal structures of a braided river aquifer. Of course it would require some scale adjustment as the scale characteristics of the site to model might differ from the scale characteristics of the successive DEMs used as TIs for the simulations. This work is going to be pursued in that direction.

Acknowledgments

The work presented in this paper is part of the ENSEMBLE project, financially supported by the Swiss National Science Foundation under the contract CRSI22 1222491. The authors would like to thank Stuart Lane

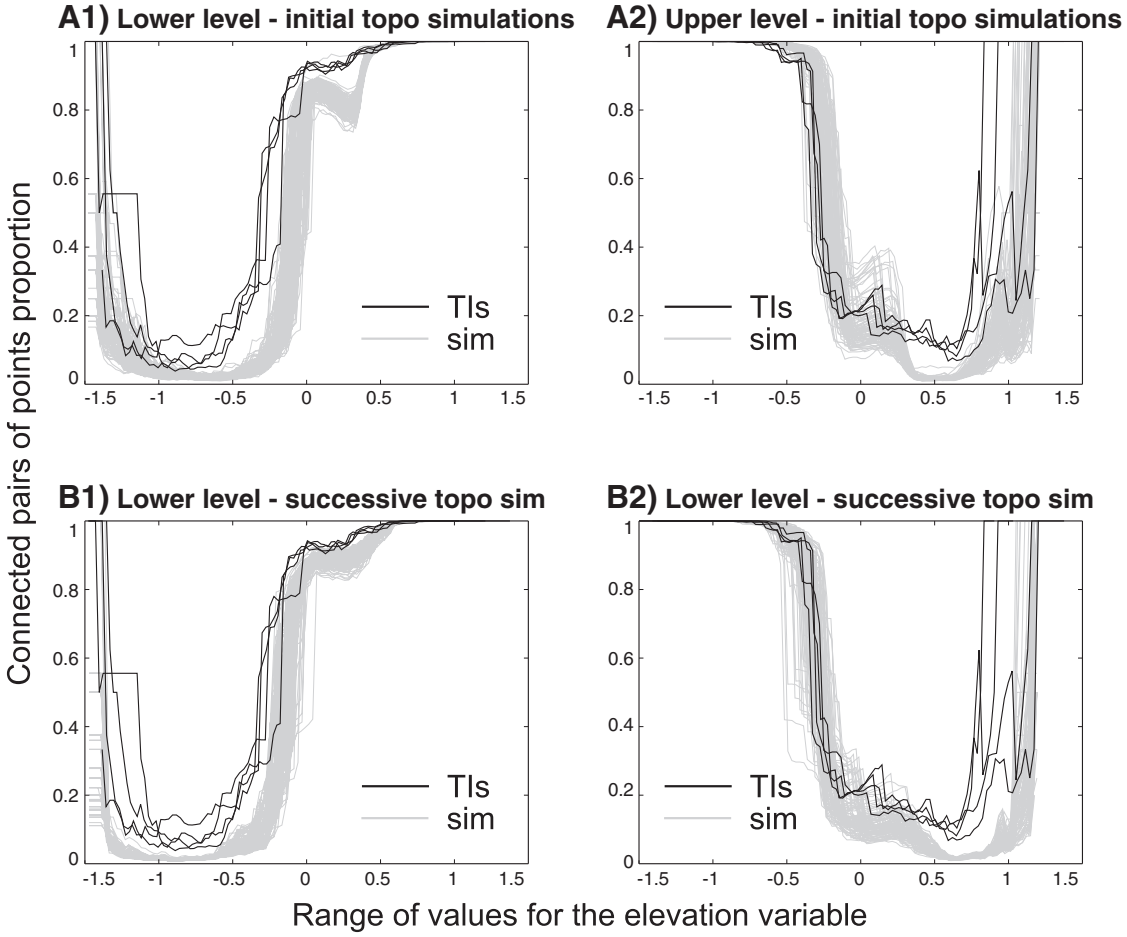

Fig. 11. Comparison of the gamma connectivities, function of the inundation threshold, betweens the TIs (black) and the simulations (gray) for cases (A) and (B), lower (1) and upper (2) levels.

for having provided the Waimakariri River data set, Gregoire Mariethoz for his constructive and motivating discussions, Michael Pyrcz for his positive review and advice, and the reviewers and the editor for their help in improving and publishing the manuscript.

References

Amoros, C., Bornette, G., 2002. Connectivity and biocomplexity in waterbodies of riverine floodplains. Freshw. Biol. 47, 761–776.

Ashmore, P., 1982. Laboratory modelling of gravel braided stream morphology. Earth Surf. Process. Landf. 7, 201–225.

Boisvert, J., Pyrcz, M., Deutsch, C., 2010. Multiple point metrics to assess categorical variable models. Nat. Resour. Res. 19, 165–175.

Boucher, A., 2009. Considering complex training images with search tree partitioning. Comput. Geosci. 35, 1151–1158.

Cao, S., Greenhalgh, S., 1994. Finite-difference solution of the eikonal equation using an efficient, first-arrival, wavefront tracking scheme. Geophysics 59, 632–643.

Chugunova, T., Hu, L., 2008. Multiple-point simulations constrained by continuous auxiliary data. Math. Geosci. 40, 133–146.

Clarke, S., Bruce-Burgess, L., Wharton, G., 2003. Linking form and function: towards an eco-hydromorphic approach to sustainable river restoration. Aquat. Conserv. Mar. Freshwater Ecosyst. 13, 439–450.

de Vries, L., Carrera, J., Falivene, O., Gratacós, O., Slooten, L., 2009. Application of multiple point geostatistics to non-stationary images. Math. Geosci. 41, 29–42.

Dimitrakopoulos, R., Mustapha, H., Gloaguen, E., 2010. High-order statistics of spatial random fields: exploring spatial cumulants for modeling complex non-gaussian and non-linear phenomena. Math. Geosci. 42, 65–99.

FOEN, S.F.O.f.t.E., 2009. Groundwater in Switzerland. URL: http://www.bafu.admin.ch/grundwasser/07496/07516/index.html?lang=en.

Foufoula-Georgiou, E., Sapozhnikov, V., 2001. Scale invariances in the morphology and evolution of braided rivers. Math. Geol. 33, 273–291.

Germanoski, D., Schumm, S., 1993. Changes in braided river morphology resulting from aggradation and degradation. J. Geol. 101, 451–466.

Glenz, D., 2013. Inverse Modeling of Groundwater Flow in the Rhône Alluvial Aquifer — Impact of the Third Rhône Correction. (Ph.D. thesis) University of Neuchâtel, Switzerland.

Goff, J., Ashmore, P., 1994. Gravel transport and morphological change in braided Sunwapta River, Alberta, Canada. Earth Surf. Process. Landf. 19, 195–212.

Gómez-Hernández, J., Wen, X., 1998. To be or not to be multi-gaussian? A reflection on stochastic hydrogeology. Adv. Water Resour. 21, 47–61.

Guardiano, F., Srivastava, R., 1993. Multivariate geostatistics: beyond bivariate moments. Geostatistics Troia 1992. Springer, pp. 133–144.

Hundey, E., Ashmore, P., 2009. Length scale of braided river morphology. Water Resour. Res. 45, W08409.

Käser, D., Graf, T., Cochand, F., McLaren, R., Therrien, R., Brunner, P., 2014. Channel representation in physically based models coupling groundwater and surface water: pitfalls and how to avoid them. Groundwater (in press).

Lane, S., 2009. Approaching the system–scale understanding of braided river behaviour. Braided Rivers. Blackwell Publishing Ltd., pp. 107–135.

Lane, S., Westaway, R., Hicks, D., 2003. Estimation of erosion and deposition volumes in a large, gravel-bed, braided river using synoptic remote sensing. Earth Surf. Process. Landf. 28, 249–271.

Macklin, M., Rumsby, B., 2007. Changing climate and extreme floods in the British uplands. Trans. Inst. Br. Geogr. 32, 168–186.

Mariethoz, G., Kelly, B., 2011. Modeling complex geological structures with elementary training images and transform-invariant distances. Water Resour. Res. 47, W07527.

Mariethoz, G., Renard, P., Straubhaar, J., 2010. The direct sampling method to perform multiple-point geostatistical simulations. Water Resour. Res. 46, W11536.

Mariethoz, G., McCabe, M., Renard, P., 2012. Spatiotemporal reconstruction of gaps in multivariate fields using the direct sampling approach. Water Resour. Res. 48, W10507.

Mariethoz, G., Comunian, A., Irarrazaval, I., Renard, P., 2014. Analog-based meandering channel simulation. Water Resour. Res. 50 (in press).

Meerschman, E., Pirot, G., Mariethoz, G., Straubhaar, J., Meirvenne, M.V., Renard, P., 2013. A practical guide to performing multiple-point statistical simulations with the direct sampling algorithm. Comput. Geosci. 52, 307–324.

Miall, A., 1977. A review of the braided-river depositional environment. Earth Sci. Rev. 13, 1–62.

Murray, A., Paola, C., 1994. A cellular-model of braided rivers. Nature 371, 54–57.

Nicholas, A., Thomas, R., Quine, T., 2009. Cellular modelling of braided river form and process. Braided Rivers: Process, Deposits, Ecology and Management (Special Publication 36 of the IAS), 21 137.

Peter, A., 2009. The Restoration of Swiss Watercourses is Urgently Necessary. URL: http://www.ethrat.ch/en/environment-sustainability/restoration-swiss-watercourses-urgently-necessary.

Peyré, G., Cohen, L., 2003. Geodesic re-meshing and parameterization using front propagation. Proc. of VLSM'03, pp. 33–40.

Pyrcz, M., Boisvert, J., Deutsch, C., 2009. Alluvsim: a program for event-based stochastic modeling of fluvial depositional systems. Comput. Geosci. 35, 1671–1685.

Renard, P., 2007. Stochastic hydrogeology: what professionals really need? Ground Water 45, 531–541.

Renard, P., Allard, D., 2013. Connectivity metrics for subsurface flow and transport. Adv. Water Resour. 51, 168–196.

Richards, K., Brasington, J., Hughes, F., 2002. Geomorphic dynamics of floodplains: ecological implications and a potential modelling strategy. Freshw. Biol. 47, 559–579.

Rust, B.R., 1972. Structure and process in a braided river. Sedimentology 18, 221–245.

Sethian, J., 1996. A fast marching level set method for monotonically advancing fronts. Proc. Natl. Acad. Sci. 93, 1591–1595.

Straubhaar, J., Renard, P., Mariethoz, G., Froidevaux, R., Besson, O., 2011. An improved parallel multiple-point algorithm using a list approach. Math. Geosci. 43, 305–328.

Straubhaar, J., Walgenwitz, A., Renard, P., 2013. Parallel multiple-point statistics algorithm based on list and tree structures. Math. Geosci. 45, 131–147.

Strebelle, S., 2002. Conditional simulation of complex geological structures using multiple-point statistics. Math. Geol. 34, 1–21.

Thomas, R., Nicholas, A., 2002. Simulation of braided river flow using a new cellular routing scheme. Geomorphology 43, 179–195.

Tockner, K., Paetzold, A., Karaus, U., Claret, C., Zettel, J., 2009. Ecology of braided rivers. In: Sambrool Smith, G.H., Best, J.L., Bristow, C.S., Petts, G.E. (Eds.), Braided Rivers: Process, Deposits, Ecology and Management. Blackwell Publishing Ltd, Oxford, UK, pp. 339–359.

Van Der Nat, D., Tockner, K., Edwards, P., Ward, J., Gurnell, A., 2003. Habitat change in braided flood plains (Tagliamento, NE-Italy). Freshw. Biol. 48, 1799–1812.

Warburton, J., Davies, T., 1994. Variability of bedload transport and channel morphology in a braided river hydraulic model. Earth Surf. Process. Landf. 19, 403–421.

Westaway, R., Lane, S., Hicks, D., 2003. Remote survey of large-scale braided, gravel-bed rivers using digital photogrammetry and image analysis. Int. J. Remote Sens. 24, 795–815.